Sliding shear capacities of the Asymmetric Friction Connection

S. Yeung, H. Zhou, H.H. Khoo & G.C. Clifton

Department of Civil Engineering, University of Auckland, Auckland.

G.A. MacRae

University of Canterbury, Christchurch.

2013 NZSEE Conference

ABSTRACT: The Sliding Hinge Joint is a beam-column connection that undergoes large inelastic rotations through sliding in Asymmetric Friction Connections. During sliding, the bolts are subject to the interaction of moment, shear and axial actions, resulting in a loss in bolt tension. The sliding shear capacities (V_{ss}) used in design are therefore based on a mathematical model developed from plastic theory, which computes the V_{ss} from the bolt size, cleat thickness (t_{cl}), coefficient of friction (μ) and lever arm between the points of bearing on the bolts (l). Prior to this research, the model had only been compared to tests limited to M24 and M30 bolts using brass shims, while abrasion resistant steel shims are used in AFC construction. This paper presents the results of 58 tests of the AFC with abrasion steel shims under SHJ rotational conditions, undertaken to determine the accuracy of the bolt model. The specimens comprised M16 to M30 bolts and t_{cl} ranging from 12 mm to 25 mm respectively. An attempt to determine μ and l experimentally was undertaken by measuring the bolt tension during sliding with a strain gauge and a load cell, and examining the impact marks on the bolts. Modifications were made to the bolt model and the recommended V_{ss} for use in design are presented.

1 INTRODUCTION

The Sliding Hinge Joint (SHJ), shown in Figure 1(a), is a low-damage beam-column connection used in moment resisting frames (MRF) (Clifton, 2005). The SHJ is rigid under working load and serviceability limit state (SLS) conditions, but allows large inelastic rotations during a major earthquake. When this occurs, the SHJ rotates about the top flange through sliding in the Asymmetric Friction Connections (AFCs) installed in the bottom web and flange bolt groups. This is achieved by a configuration where the beam top flange is connected to the column by a conventional bolted connection whilst the bottom beam flange and bottom web are connected by AFCs. This configuration forces the beam to rotate about an effective pin at the beam top flange during a major earthquake, while dissipating energy through friction. Figure 1(b) illustrates the components in the bottom flange AFC. Horizontally slotted holes in the cleat form a slotted bolted connection to allow sliding during a major earthquake, dissipating energy and minimising damage to the structural frame. The AFC plates are clamped together by a group of Property Class 8.8 steel bolts, which are fully tensioned to the turn-of-nut method in accordance with NZS 3404:1997 (Standards New Zealand 1997).

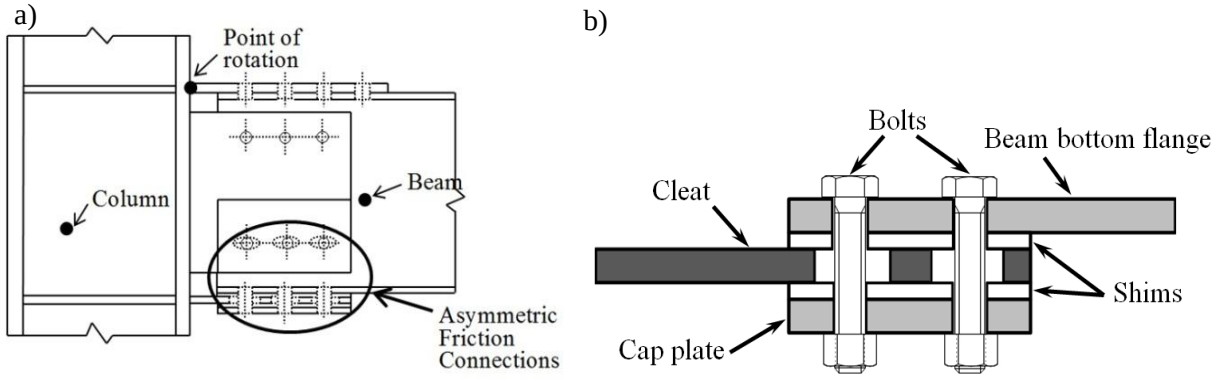

Figure 1. (a) Sliding Hinge Joint (MacRae et al. (2010)) and (b) Asymmetric Friction Connection

There are two sliding surfaces in the AFC, namely: (1) the interface between the upper shim and the beam bottom flange, and (2) the interface between the lower shim and the cleat. Figure 2(a) shows the AFC idealised force-displacement behaviour. As the seismic demand exceeds the frictional resistance of the AFC, sliding first occurs on the first interface as shown by *A* in Figure 2(a). Further increases in seismic demand forces the second interface to slide, which is represented by *B*. At this stage, the bolt is in double curvature with bending moment distribution shown in Figure 2(b). This is further described in Section 1.2. Upon load reversal, sliding occurs on the first interface (*C*), followed by the second interface (*D*).

Current recommendation for the SHJ uses Grade 400 abrasion resistant steel shims (Khoo et al., 2012a). However, there is a lack of experimental data on this setup, which is required to further enhance our understanding of the connection behaviour. The objective of this study was to provide more reliable V_{ss} for use in design by increasing the experimental database and improving the bolt model, the latter of which was attained by determining more reliable input parameters. This paper was written to answer the following questions:

1. How does the bolt behave during sliding?
2. What are the recommended input parameters in the bolt model to compute the predicted V_{ss}?
3. How representative is the model of the experimentally measured V_{ss}?

1.1 Sliding shear capacity (V_{ss})

The V_{ss} is the AFC design sliding shear capacity (kN/bolt), measured when the AFC is in the stable sliding state. The V_{ss} is a function of the installed bolt tension (N) and the coefficient of friction between the sliding surfaces (μ). Consequently, the friction equation is adopted for determining the V_{ss}, as given in Equation 1, where V_{ss} is the sliding shear capacity, μ is the coefficient of friction and N is the bolt tension. The factor of two accounts for the two surfaces in sliding. As different bolt sizes are associated with different installed bolt tension, the V_{ss} is determined for a range of bolt sizes for use in design. These values are predicted by the mathematical bolt model developed by Clifton (2005) and modified by MacRae et al. (2010) and is described in the following section.

1.2 Bolt model

Experimental tests showed that once the joint is forced into the sliding state, the AFC bolts lose installed tension and is associated with a decrease in the V_{ss}. This is because the AFC bolts are subjected to a moment, shear and axial force (MVP) interaction from bending in double curvature during joint sliding (Fig. 2b). This causes an uneven stress distribution through the bolt cross sectional area and results in a reduced bolt tension to that initially installed. The V_{ss} is therefore computed by an MVP interaction model developed from plastic theory by Clifton (2005). The moment lever arm (l), coefficient of friction (μ) and bolt size were the required inputs into the bolt model to calculate the final sliding shear resistance. The bolt model was later modified by MacRae et al. (2010), and shown in Equations 1-6.

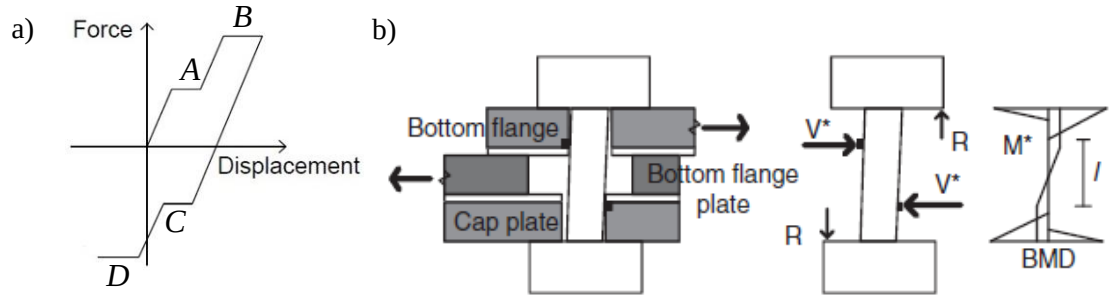

Figure 2. Idealised (a) force-displacement curve (Khoo et al. (2012a)) and (b) bolt behaviour during sliding (Khoo et al. (2012a))

$$V_{ss} = 2\mu N \quad (1)$$

$$\left(\frac{M^*}{M_{rfn}}\right) + \left(\frac{V^*}{V_{fn}}\right) = 1 \quad (2)$$

$$V^* = N\mu \quad (3)$$

$$M^* = \frac{V^* l}{2} = \frac{N\mu l}{2} \quad (4)$$

$$M_{rfn} = S_{fn}\left(1 - \left(\frac{N}{N_{tf}}\right)^c\right) f_{uf} \approx 0.1665 d^3 (1 - \left(\frac{N}{0.56 d^2 f_{uf}}\right)^c) f_{uf} \quad (5)$$

$$V_{fn} \approx 0.62 f_{uf} \times 0.56 d^2 \quad (6)$$

where: M^* = bolt moment demand; M_{rfn} = bolt moment capacity with axial force interaction; V^* = bolt shear demand; V_{fn} = bolt shear capacity with axial force interaction; N = bolt tension during sliding; μ = coefficient of friction between sliding surfaces; l = lever arm between points of bearing on bolt; S_{fn} = plastic section modulus of bolt core; N_{tf} = nominal tension capacity of a bolt; f_{uf} = ultimate tensile stress of bolt; c = constant taken as 1 or 2, with or without Belleville Springs; d = nominal bolt diameter.

The bolt model predicts a trend of decreasing V_{ss} with increasing l. Comparisons of the bolt model V_{ss} with experimental tests by Clifton (2005) and Khoo et al. (2012a) showed that this trend was observed within the results of each bolt size. It was also found that the smaller M16 and M20 bolts developed disproportionately higher V_{ss} compared to M24 and M30 bolts, which indicated an apparent bolt size effect not accounted for in the bolt model.

During joint sliding, steel plates of the AFC bear on the bolts in two locations as shown in Figure 2(b). The locations of impact determine the l, which influences the bending moment and consequently the MVP interaction of the bolts. The observed impact locations on the bolts during AFC sliding differed between researchers. The bearing location for design was assumed to be at the cap plate and beam flange locations by Clifton (2005) and MacRae et al. (2010). However, visual evidence from tests performed by Khoo et al. (2012b) indicated that the initial bearing locations were at the shims. The μ used in the bolt model for steel against steel was 0.35 as recommended by Grigorian and Popov (1994). This was based on tribology studies of coefficient of friction values for slip-critical joints, and may not be valid for the current SHJ configuration.

2 TEST DESCRIPTION

2.1 Test setup

The test setup (Fig. 3a) replicated the AFC in the bottom flange plate. It consisted of a reaction arm hinged to a strong wall at A, an actuator applying load at B, and the AFC specimen at C. The rotational movement was produced by an actuator applying a load at the base of the reaction arm at B, resulting in a rotational motion about the hinge at A. This produced a relative displacement between the cleat and the plates at the top of the reaction arm, which is similar to actual AFC bottom flange

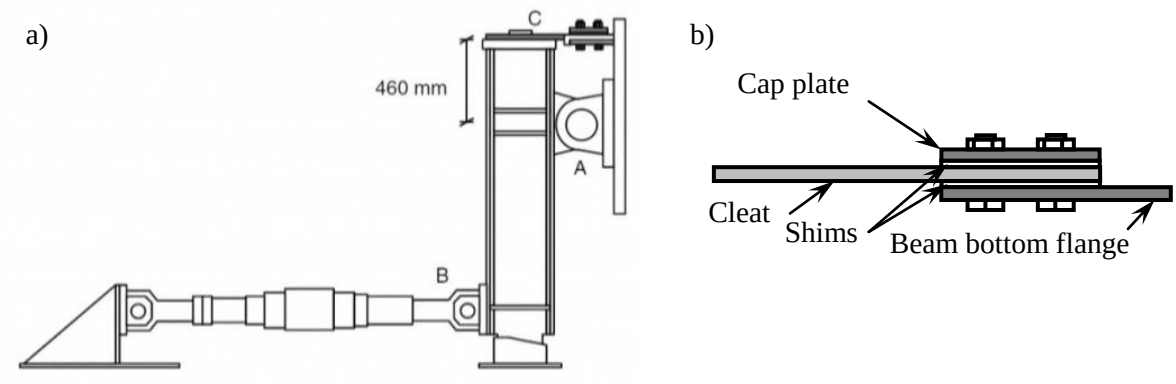

Figure 3. (a) Test setup (Khoo et al. (2012a)) and (b) AFC configuration during testing

behaviour. The test setup amplified the actuator load by a factor of 2.33. The distance between the hinge at A and the bottom flange at C was 460mm, corresponding to a SHJ with a 460UB section beam. This formed an inverted SHJ configuration (Fig. 3b). An internal load cell in the actuator measured the applied load at point B which was multiplied by 2.33 to obtain the V_{ss} of the joint. Displacement gauges were installed at C to measure the relative displacement between the cleat and beam flange during sliding.

2.2 **Test specimens**

A total of 35 tests were performed, comprising bolt size and flange plate thickness combinations shown in Table 1. The results were analysed with results from Khoo et al. (2012a), giving a total of 58 values. The shims used for testing were 5mm thick Grade 400 abrasion resistant steel shims. A bolt group of four bolts were used in all tests, and were fully tensioned to a third of a turn in the part turn method in accordance with NZS3404:1997 (Standards New Zealand 1997).

The effect of bearing location on V_{ss} was determined by testing M20 bolts of 120 mm length with either (1) both bearing locations at the shank or (2) one bearing location and the threaded region and one bearing location at the shank. The bearing location was altered between (1) and (2) by the placement of washers either adjacent to the bolt head or adjacent to the nut so that the bearing components impact on the intended location. After each test, the bolts were visually inspected for indentations to determine the lever arm length.

The coefficient of friction was determined by testing 110 mm long M20 bolts with strain gauges installed inside the bolt shank and washer-type load cells simultaneously installed under the bolt head. The bolts were tested at the two bolt row locations, namely the row closer to the reaction arm and the row further from the reaction arm. This allows prying effect to be investigated.

2.3 **Loading regime**

The AFC specimens were subjected to a dynamic loading regime with increasing cycles of sine wave loading. The target joint rotation was 30 mrad, corresponding to 13.8 mm of horizontal displacement at the AFC, based on the demands expected in a typical MRF (SAC Joint Venture, 2000). In reality, the target displacements were not achieved due to flexibility of the reaction arm and slippage between the components and rig. This effect was accounted for in the adopted loading regime, resulting in an average peak displacement of 14 mm. The loading was applied at a frequency of 0.67 Hertz.

2.4 **Bolt tension measurements**

Real time monitoring of the bolt tension during sliding tests was used to determine the μ between Grade 400 abrasion resistant steel shims and Grade 300 steel plates. Two methods of bolt tension measurement were adopted, namely (1) washer type load cells and (2) strain gauges installed within the bolt shank (Fig. 4).

The load cells were placed within the grip length of the bolt to measure the clamping force of a bolt. The load cell model was LWO-60 with a maximum compressive load of 267 kN (Transducer

Table 1. Test specimens

Bolt size	**Cleat thickness (t_{cl}) (mm)**	**Number of tests**
M16	12	3
	16	2
M20	12	3
	16	15
	20	6
M24	16	3
	20	3

Techniques Company Limited, 2012). The load cells were positioned between the bolt head and the beam flange to minimise uneven stress distribution on the load cell caused by bolt bending and to avoid instrument damage from sliding movements.

The strain gauge model was KFG-1.5-120-C20-11 and was installed with EP-180 adhesive (Kyowa Electronic Instruments Company Limited, 2012). The strain gauges were installed inside a 2mm diameter hole drilled along the longitudinal axis of the bolt from the bolt head to the shank-thread intersection (Fig. 4). The strain gauge was positioned halfway into the drilled hole to avoid the effects of 'strain spreading' at the shank-thread intersection and the shank-bolt head intersection from affecting the tension readings. 'Strain spreading' is the change in strain associated with a change in cross section area at the shank-head interface and the shank-thread interface. The hole was sealed with adhesive following strain gauge placement.

3 RESULTS AND DISCUSSION

3.1 Sliding shear resistance

The hysteresis curve in Figure 5 shows the sliding behaviour of the AFC. The sliding behaviour was characterised by an initial stabilisation in strength associated with the first surface in sliding during small-amplitude loading. Further increases in loading forces the second surface to slide and is shown by the stabilisation at maximum strength.

Figure 6 compares the 58 test values of V_{ss} with l, normalised by the bolt proof load and bolt diameter respectively. The average V_{ss} for each bolt size and t_{cl} combination is also displayed. A trend of decreasing V_{ss} with increasing t_{cl} was observed for all three bolt sizes. This trend is consistent with the bolt model. However, M16 bolts showed less of a decrease in V_{ss} with increasing lever arm when compared with M20 and M24 bolts. This could be due to the variability in bolt material properties and variations in installed tension. While a minimum tensile proof load is expected during full-tensioning, the actual installed bolt tension is generally higher and can vary by a significant margin, which causes variability in strengths of the connection. The unexpected M16 results may also be due to the smaller sample size of 11.

There was an observed difference in strength between loading in the positive and negative direction (Fig. 5). Positive loading is associated with the beam bottom flange rotating towards the cleat and negative loading is associated with the beam bottom flange rotating away from the cleat. The V_{ss} for negative loading was consistently higher than positive loading. Negative loading V_{ss} was on average 10 kN higher than V_{ss} for positive loading, and is on average 22% higher.

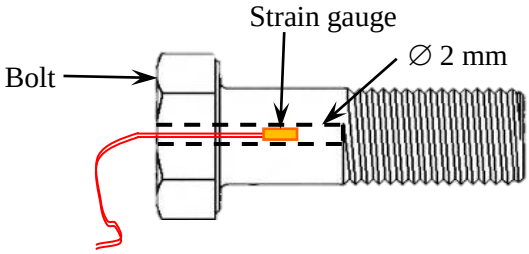

Figure 4. Strain gauge in bolt

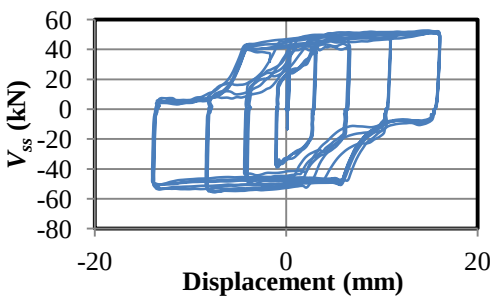

Figure 5. Hysteresis curve for M16 bolts and 16 mm cleat

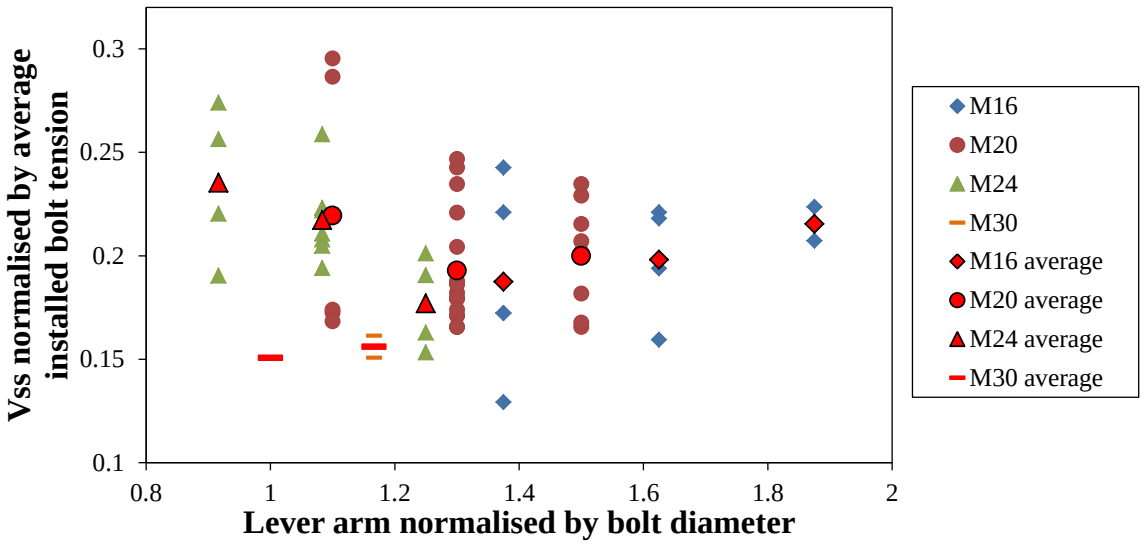

Figure 6. Scatter plot of normalized V_{ss} against normalized lever arm

3.2 Coefficient of friction

The μ was calculated with $\mu = V_{ss}/2N$ where: V_{ss} was the sliding shear force measured by a load cell in the dynamic actuator and N was the measured bolt tension from the strain gauge installed in the bolt. The washer-type load cell readings are not discussed herein due to the relative unreliability of the load cell readings. Further information can be found in Khoo (2013).

The μ was determined for the final five cycles of loading at maximum amplitude and taken at the instant the reaction arm was vertical in order to prevent prying effects from affecting bolt tension readings. Figure 7 is an example of the plot of μ against displacement for the final five cycles of loading. The plot presents the μ obtained from both positive and negative loading. Stable sliding was observed at the horizontal sections at points A and B, therefore the μ values are only valid at these locations. The μ was taken at displacement = 0 which corresponds to the vertical position of the reaction arm. The final design coefficient of friction was the average between the two loading directions and averaged between the two bolt rows tested.

The average μ for positive loading was 0.47 and the average μ for negative loading was 0.50. The 10^{th} percentile and 90^{th} percentile coefficient of friction was 0.43 and 0.58, respectively. The average nominal μ was 0.48. This value is significantly higher than the adopted tribology value of 0.35 for steel against steel sliding. The recommended μ for use in design is therefore 0.48. However, further tests should be performed to determine the μ for more samples and for different bolt sizes.

3.3 Bolt lever arm

The bolt lever arm previously adopted was taken as t_{cl} + *shim thickness* (t_{sh}) as a result of visual evidence of shim impact locations from Khoo et at. (2012b). However, the component tests in this study indicated that the cap plate and bottom flange plate were also hitting the bolt. Approximately half of the tests had a bearing location at the cap plate and the beam flange, with the other half bearing at the shims. This visual evidence suggested that the bolt lever arm is larger than what was recommended by Khoo et al. (2012b), but smaller than the lever arm described by Clifton (2005) and MacRae et al. (2010). The points of bearing were at the cap plate and bottom beam flange in one direction of sliding and at the top and bottom shims in the opposite direction (Fig. 8). To account for this behaviour, the two points of bearing were allocated as the average hitting locations between both loading directions. The lever arm shall therefore be taken as the distance from the shim/cap plate interface to the shim/bottom flange interface. The proposed new lever arm equation is $l = t_{cl} + 2t_{sh}$.

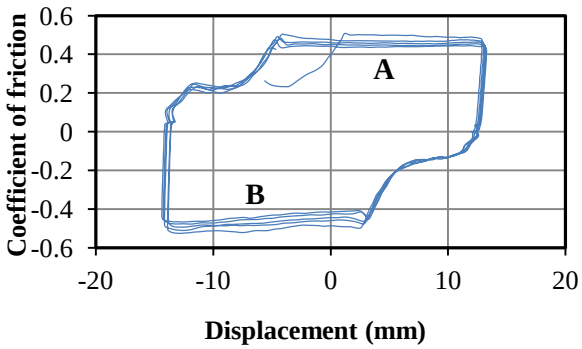

Figure 7. Coefficient of friction for M20 bolt and 20mm cleat

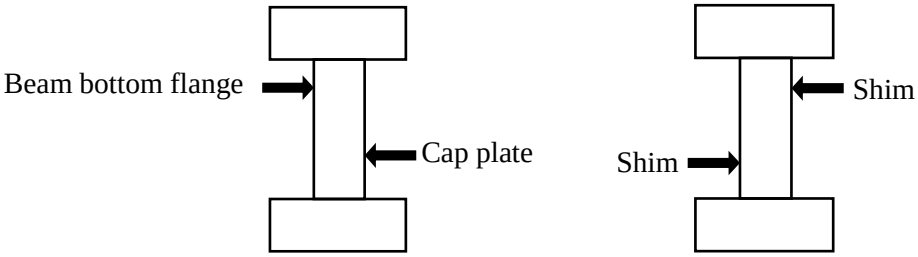

Figure 8. Observed bearing locations

3.4 **Bearing locations**

The bearing locations for each bolt were examined and recorded for M16, M20 and M24 bolts during the course of experimental testing. For each different bolt size, the hitting locations were consistent amongst specimens of the same bolt and cleat size. The bearing location on M16 and M20 bolts were on the shank for both hitting locations. For the M24 bolts, the impact location was on the shank for the head side, and on the threads for the nut side.

The previous bolt model equations assumed that each bolt had both hitting locations at the shank. Visual evidence showed that this was applicable for M16 and M20 bolts. However, M24 bolts had one of its hitting locations at the shank and the other at the thread. The smaller cross sectional area at the threads reduces the V_{ss}, leading to an overestimation of joint strength for larger bolt diameters. This is a possible cause of the bolt size effect where smaller diameter bolts produce proportionately larger V_{ss}.

Consequently, a modification to the bolt model is proposed. In order to incorporate this finding into the model, it is proposed that Equations 7-9 are applied for M24 and M30 bolts in conjunction with Equations 2-6. These equations take into account the actual location on the bolt that generates the shear and moment capacities, producing more representative predictions.

$$M_{rf,thread} = S_{f,thread}\left(1-\left(\frac{N}{N_{tf,thread}}\right)^{c}\right)f_{uf}$$
$$\approx 0.1665{d_{thread}}^{3}\left(1-\left(\frac{N}{0.56{d_{thread}}^{2}f_{uf}}\right)^{c}\right)f_{uf} \quad (7)$$

$$V_{f,thread} \approx 0.62f_{uf} \times 0.56{d_{thread}}^{2} \quad (8)$$

$$\left(\frac{2M^{*}}{M_{rf}+M_{rf,thread}}\right)+\left(\frac{2V^{*}}{V_{f}+V_{f,thread}}\right) = 1 \quad (9)$$

Where: $M_{rf,thread}$ = bolt moment capacity at the threads with axial force interaction; $S_{f,thread,}$ = plastic section modulus of the minor diameter; $N_{tf,thread}$ = nominal tension capacity of the threads; d_{thread} = minor diameter; $V_{f,thread}$ = bolt shear capacity at the threads with axial force interaction; and all other variables as for Equations 2-6.

4 BOLT MODEL VALIDATION

Figure 9(a) and (b) compares the experimental results with the revised bolt model and the bolt model from MacRae et al. (2010), respectively. The latter incorporated the following input parameters: μ = 0.35, $l = t_{cl}+2t_{sh}+ 0.2\times bolt\ diameter$, 5th percentile UTS and proof load specified in NZS 3404:1997.

The average ultimate tensile strength (UTS) was used as input into the revised bolt model as bolts are generally stronger than the specified strengths. Therefore 930 MPa was used in f_{uf}, which is 830×1.12, where 830 MPa is the UTS and the factor of 1.12 increases the UTS to the average strength (Clifton, 2005). The average installed bolt tension was used in place of the specified minimum proof load for the same reasons. These are 116 kN, 181 kN and 261 kN for M16, M20 and M24 bolts, respectively. The μ was taken as 0.48 from testing. The V_{ss} was calculated from Equations 2-9.

The scatter of the experimental data was large. This was due to variations in bolt material properties, sliding surface conditions and installed bolt tension. Observation of experimental data points gave visual verification that V_{ss} decreased with increasing l. This is due to the increased bolt bending moment associated with increasing l which in turn reduces bolt tension from the increased MVP effect. As the amount of bolt tension retained in each bolt decreased, V_{ss} also reduced.

The predictions from both bolt models were a close match to the experimental data points. Both models produced similar predictions for M16 and M20 bolt diameters, with the revised bolt model predicting a lower V_{ss} for all bolt sizes. The revised bolt model produced more representative estimates of V_{ss} for M24 and M30 bolts. This is shown by the reduced V_{ss} for the shorter lever arm lengths in Figure 9(a), which fits the experimental trend observed for larger bolt diameters. The revised bolt model equations are therefore adequate for predicting the V_{ss} for varying bolt size and lever arm.

An overstrength factor (ϕ_o) of 1.4 was applied to the bolt model predictions as determined from MacRae et. al (2010), and shown in Figure 9(a) and (b). The revised bolt model had two data points with measured strength above the ϕ_o factored bolt model predictions, while the bolt model from MacRae et al. (2010) had no outliers. A majority of the data points had a strength level above the bolt model predicted strength after the incorporation of the strength reduction factor (ϕ) of 0.7. The revised bolt model had 1 data point with V_{ss} outside the ϕ factored predictions, whereas the MacRae et al. (2010) bolt model had 4 data points.

The design values for the V_{ss} as calculated from the revised bolt model are shown in Table 2. These capacities are computed for 5mm thick Grade 400 hardness shims. A strength reduction factor (ϕ) of 0.7 is recommended to take the variability of the experimental bolt strengths into account.

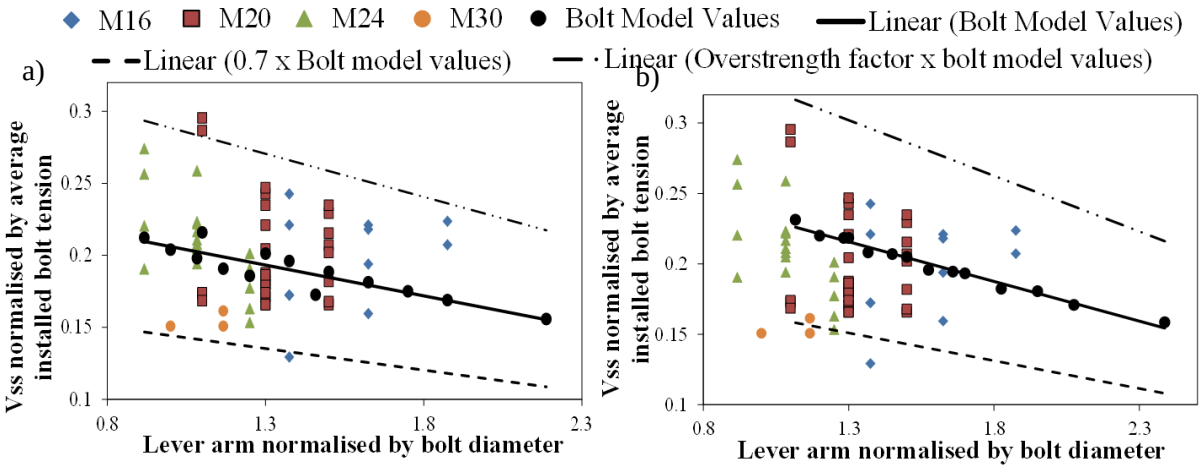

Figure 9. (a) Experimental V_{ss} with revised bolt model predictions and (b) experimental V_{ss} with MacRae et al. (2010) bolt model predictions

Table 2. ϕV_{ss} design values, in kN

Bolt size	Cleat thickness (mm)			
	12	**16**	**20**	**25**
M16	32	29	27	25
M20	55	51	48	44
M24	78	72	68	63
M30	-	-	118	111

5 CONCLUSIONS

1. The bolt is characterised by an initial loss of tension at commencement of sliding, followed by an increase in tension which stabilised as the bolt underwent bending. The V_{ss} increased with increasing bolt diameter, and reduced with increasing cleat thickness. The observed bolt size effect was likely caused by a difference in bearing location on the bolt shaft. This effect was accounted for in the proposed revision to the bolt model equations.
2. The lever arm should be calculated as $l = 2t_{sh} + t_{cl}$ and $\mu = 0.48$ is recommended. The bolt diameter used in the bolt model should be taken as the shank diameter for M16 and M20 bolts, and the average of the shank and thread diameter for M24 and M30 bolts.
3. The bolt model predicted values matched the experimental data points well and were therefore adequate for predicting the V_{ss} of SHJ setups with varying bolt sizes and t_{cl}. However, the scatter of data points was large due to variability of material properties. A strength reduction factor of 0.7 is therefore recommended to take this into account.

6 REFERENCES

Clifton, G. C. 2005. *Semi-rigid joints for moment-resisting steel framed seismic-resisting systems.* PhD Thesis, University of Auckland.

Grigorian, C. E. & Popov, E. P. 1994. Energy dissipation with slotted bolted connections. *Earthquake Engineering Research Center*. Berkeley, California: University of California at Berkeley.

Khoo, H. H. 2013. *Development of the low-damage self-centering Sliding Hinge Joint.* PhD Thesis, University of Auckland.

Khoo, H. H., Clifton, G. C., Butterworth, J. W. & MacRae, G. A. 2012a. Shim and bolt size effects on the Asymmetric Friction Connection. *7th STESSA Conference on Behaviour of Steel Structures in Seismic Areas.* Santiago, Chile.

Khoo, H. H., Clifton, G. C., Butterworth, J. W., MacRae, G. A. & Ferguson, G. 2012b. Influence of steel shim hardness on the Sliding Hinge Joint performance. *Journal of Constructional Steel Research,* 72**,** 119-129.

Kyowa Electronic Instruments Company Limited 2012. KFG Strain Gauge. Tokyo, Japan.

MacRae, G. A., Clifton, G. C., Mackinven, H., Mago, N., Butterworth, J. W. & Pampanin, S. 2010. The Sliding Hinge Joint Moment Connection. *Bulletin of New Zealand Society of Earthquake Engineering,* 43**,** 202-212.

SAC Joint Venture 2000. Recommended design criteria for new steel moment frame structures. Washington, D.C.

Standards New Zealand 1997. NZS 3404:1997 Incorporating Amendmend No.1 and Amendment No. 2. Wellington, New Zealand: Standards New Zealand.

Transducer Techniques Company Limited. 2012. *LWO Load Cells* [Online]. Rio Nedo, Temecula, California.